International Journal of Pharmaceutics: X 6 (2023) 100206

Contents lists available at ScienceDirect

International Journal of Pharmaceutics: X

journal homepage: www.sciencedirect.com/journal/international-journal-of-pharmaceutics-x

Novel nasal niosomes loaded with lacosamide and coated with chitosan: A possible pathway to target the brain to control partial-onset seizures

Alaa S. Tulbah [a], Mohammed H. Elkomy [b,*], Randa Mohammed Zaki [c,d], Hussein M. Eid [d,*], Essam M. Eissa [d], Adel A. Ali [d], Heba A. Yassin [e], Basmah Nasser Aldosari [f], Ibrahim A. Naguib [g], Amira H. Hassan [d]

[a] Department of Pharmaceutics, College of Pharmacy, Umm Al-Qura University, Makkah 21955, Saudi Arabia
[b] Department of Pharmaceutics, College of Pharmacy, Jouf University, Sakaka 72341, Saudi Arabia
[c] Department of Pharmaceutics, College of Pharmacy, Prince Sattam Bin Abdulaziz University, P.O. Box 173, Al-Kharj 11942, Saudi Arabia
[d] Department of Pharmaceutics and Industrial Pharmacy, Faculty of Pharmacy, Beni-Suef University, Beni-Suef 62511, Egypt
[e] Department of Pharmaceutics and Industrial Pharmacy, Faculty of Pharmacy, Sinai University (Arish campus), Arish, Egypt
[f] Department of Pharmaceutics, College of Pharmacy, King Saud University, P.O. Box 2457, Riyadh 11451, Saudi Arabia
[g] Department of Pharmaceutical Chemistry, College of Pharmacy, Taif University, P.O. Box 11099, Taif 21944, Saudi Arabia

ARTICLE INFO

Keywords:
Intranasal
Pharmacokinetics
Nose-to-brain delivery
Focal seizures
Antiepileptic
Chitosomes
Mucoadhesive

ABSTRACT

This work aimed to develop and produce lacosamide-loaded niosomes coated with chitosan (LCA-CTS-NSM) using a thin-film hydration method and the Box-Behnken design. The effect of three independent factors (Span 60 amount, chitosan concentration, and cholesterol amount) on vesicle size, entrapment efficiency, zeta potential, and cumulative release (8 h) was studied. The optimal formulation of LCA-CTS-NSM was chosen from the design space and assessed for morphology, in vitro release, nasal diffusion, stability, tolerability, and in vivo biodistribution for brain targeting after intranasal delivery. The vesicle size, entrapment, surface charge, and in vitro release of the optimal formula were found to be 194.3 nm, 58.3%, +35.6 mV, and 81.3%, respectively. Besides, it exhibits sustained release behavior, enhanced nasal diffusion, and improved physical stability. Histopathological testing revealed no evidence of toxicity or structural damage to the nasal mucosa. It demonstrated significantly more brain distribution than the drug solution. Overall, the data is encouraging since it points to the potential for non-invasive intranasal administration of LCA as an alternative to oral or parenteral routes.

1. Introduction

Epilepsy is a highly prevalent neurological illness that affects millions of individuals worldwide (Organization, 2019). It is marked by epileptic seizures, which happen when an alteration in the brain's normal electrical activity (Musumeci et al., 2019). Various seizure types have many clinical symptoms, including partial or total cognitive impairment (Pires et al., 2021). Therapy varies depending on the type of seizure and other factors that can affect it, such as age, side effects, and the use of other drugs simultaneously. Depressive disorders, anxiety disorders, intellectual disability, learning difficulties, and autism are among the comorbidities that may occur with epilepsy (Musumeci et al., 2019). Until now, no therapy has been demonstrated to cure epilepsy. Thus, pharmaceutical therapy focuses on symptom management through persistent use of antiepileptic medicines.

Lacosamide (LCA) stands out from all other antiepileptic medications on the market owing to its two innovative modes of action, safety characteristics, and superior pharmacokinetics. LCA preferentially promotes the delayed inactivation of voltage-gated sodium channels (VGSCs), unlike traditional VGSC modulators such as phenytoin, oxcarbazepine, and carbamazepine (de Biase et al., 2014). The modulation of slow inactivation of VGSCs by LCA selectively stabilizes hyperexcitable neuronal membranes, decreasing repetitive neuronal firing. As a result, LCA decreases the pathological hyperactivity that underpins epilepsy while not affecting physiological activity (Halford and Lapointe, 2009). In addition, LCA reduces collapsing-response mediator

* Corresponding authors.
E-mail addresses: astulbah@uqu.edu.sa (A.S. Tulbah), mhalkomy@ju.edu.sa (M.H. Elkomy), hussien.eid@pharm.bsu.edu.eg (H.M. Eid), essam.mohamed@pharm.bsu.edu.eg (E.M. Eissa), adel.ali@pharm.bsu.edu.eg (A.A. Ali), Heba_Ahmed@buc.edu.eg (H.A. Yassin), baldosari@ksu.edu.sa (B.N. Aldosari), i.abdelaal@tu.edu.sa (I.A. Naguib), amira.abdelatef@pharm.bsu.edu.eg (A.H. Hassan).

https://doi.org/10.1016/j.ijpx.2023.100206
Received 11 May 2023; Received in revised form 9 August 2023; Accepted 11 August 2023
Available online 12 August 2023

protein-2, diminishing neurotrophic factors effects and suppressing spontaneous recurring seizures, hence inhibiting epileptogenesis (Wang et al., 2018). This feature is unique to LCA (Engel Jr and Pitkänen, 2020). LCA has been used in various disorders, including the treatment of chronic migraine (Lionetto et al., 2012), diabetic patients (Carmland et al., 2019; Moutal et al., 2016), hypoxic-ischemic brain injury (Kim et al., 2017), inflammation (Al-Massri et al., 2018), and glioma (Rizzo et al., 2017). LCA also has a dose-proportional pharmacokinetic profile, negligible first-pass hepatic metabolism, low plasma protein binding, and high intestinal absorption (Gonçalves et al., 2021). However, it is a substrate of P-glycoprotein (P-gp) (Zhang et al., 2013), which is highly expressed in refractory epilepsy (Lazarowski et al., 2007). As a result, the amount of LCA that can cross the BBB is anticipated to diminish as the illness worsens and the P-gp expression rises.

LCA is marketed in several dosage forms, such as syrups and tablets for oral use, and intravenous infusion solutions. Parenteral administration is advantageous for hospitalized patients, patients having trouble swallowing, and patients experiencing acute gastrointestinal issues. However, intravenous injections are intrusive and need trained medical experts. The oral route is the most often used for long-term therapy; however, the patient during the epileptic episode may experience nausea or vomiting (Musumeci et al., 2019). In addition, GIT disturbances are among the most common side effects of LCA (Halford and Lapointe, 2009). Thus, it is crucial to offer an alternative dosage form that the patient may administer to enhance the quality of life for those with epilepsy (Amengual-Gual et al., 2019).

The intranasal pathway has received much interest as a non-invasive way to quickly deliver medications to blood circulation and the brain (Eissa et al., 2022; Elkomy et al., 2022b; Elkomy et al., 2023). This is due to the large surface area and adequate blood flow of nasal mucosa. Additionally, nasal mucosa olfactory cells extend into the brain cavity (Abo El-Enin et al., 2022). When a nasal drug delivery system contacts the mucosa, the medication bypasses the BBB and is transmitted directly to the brain, producing an immediate effect (Eid et al., 2019b; Elkomy et al., 2022b). However, the intranasal route is limited by quick mucociliary washout, low instillation volume, and poor absorption of hydrophilic molecules (Elsenosy et al., 2020). Several previous research assessed the efficacy of the nose-to-brain (NTB) route in controlling seizures (Costa et al., 2019; Gangurde et al., 2019; Musumeci et al., 2018; Salama et al., 2021).

Niosomes (NSM) are vesicular structures comprised of cholesterol and non-ionic surfactants. Although NSM has a structure comparable to liposomes, NSM is more stable and cost-effective (Eid et al., 2021; Kazi et al., 2010). The unique features of NSM, such as increasing penetration across biological membranes, stability, and drug solubility, have been extensively investigated for various routes of administration. Insufficient drug absorption occurs due to mucociliary clearance, which dramatically reduces the time nanoparticles remain in the nasal cavity (Abo El-Enin et al., 2022). Chitosan (CTS) has been regarded as an efficient biodegradable polymer for drug delivery because of its improved mucoadhesion, enzyme inhibition, P-gp inhibition, and augmentation of permeability by opening the epithelium's tight junctions (Abo El-Enin et al., 2022; Sohail et al., 2019). CTS also has a high level of biocompatibility and minimal toxicity.

Herein, we formulated and characterized lacosamide-loaded niosomes coated with chitosan (LCA-CTS-NSM) for LCA delivery to the brain via the intranasal pathway. This is the first study investigating the efficacy of CTS surface modified NSM as an intranasal delivery system for LCA brain targeting. The physical and morphological features of LCA-CTS-NSM were evaluated to ensure their suitability for brain targeting. Lastly, the safety and biodistribution of LCA-CTS-NSM and LCA solution (LCA-SOL) following intranasal administration were assessed.

2. Materials and methods

2.1. Materials

Lacosamide powder (LCA) was obtained as a gift from Marcyrl Company (Cairo, Egypt). Span 60, Cholesterol, Methanol (HPLC grade), Dialysis membrane (MW cut off: 12000 Da), Chitosan (low MW), Acetonitrile (HPLC), and Chloroform (HPLC) were purchased from Sigma-Aldrich (St. Louis, MO). The other substances used were of analytical grade.

3. Methods

3.1. Experiment design and optimization

The optimized formulation was developed through Design-Expert Software (12.0.3.0, Stat-Ease Inc., USA). The trials were designed using three independent variables (Span 60 amount, cholesterol amount, and CTS concentration), as shown in Table 1, with Span 60 ranging from 40 to 120 mg, cholesterol ranging from 15 to 30 mg, and CTS concentration ranging from 0.1 to 0.4%. The dependent variables chosen for the formulation were vesicle size (VS), zeta potential (ZP), entrapment efficiency (EE), and cumulative release after 8 h (CR). Based on this, 16 different runs (12 formulations and 4 repeated central points) were designed using Box Behnken design (BBD). 3D surface graphs are plotted in the R program using the plot3D package (Panda et al., 2021; Soetaert, 2017). The optimization constraints were designed to maximize ZP, EE, and CR and minimize VS (Eid et al., 2022; Elkomy et al., 2022c).

3.2. HPLC assay

A validated HPLC method was used to estimate the quantity of LCA (Gonçalves et al., 2021). The Agilent Eclipse —C_{18} column (5 µm PS, i.d., 4.60 mm × 25 cm) was used. The mobile phase of the HPLC system was pumped with acetonitrile and water at a ratio of 90:10 (*v*/v) with a 1 mL/min flow rate. The column temperature, the UV detection, and the injection volume were 40 °C, 220 nm, and 20 µL, respectively. The proposed HPLC method generated a linear calibration curve covering the concentration range of 0.1–1 µg/mL (R^2 = 0.998). The limit of detection (LOD) and the limit of quantitation (LOQ) were 0.033 µg/mL, and 0.1 µg/mL, respectively.

3.3. Formulation of LCA-CTS-NSM

The lacosamide-loaded niosomes (LCA-NSM) were formulated via thin-film hydration (Eid et al., 2021; Elkomy et al., 2022d). In a nutshell, Span 60 and cholesterol were mixed into chloroform: methanol combination (15 mL, 2:1 v/v). A rotary evaporator (Stuart rotary evaporator, United Kingdom) was used to evaporate the organic solvents at a temperature of 55 °C, forming a thin film. The developed thin film was hydrated by adding 10 mL phosphate buffered saline (pH 7.4) containing 10 mg LCA, then sonicated for 30 min (Eid et al., 2021). CTS solution was formulated by dissolving it in 1% glacial acetic acid. The LCA-CTS-NSM was prepared by adding CTS solution dropwise to the prepared niosomal dispersion under magnetic stirring. The stirring speed was 100 rpm, and the drop rate was 0.2 mL/min. The final preparation was stored in the refrigerator for subsequent investigation. Table 1 displays the constituents of the LCA-CTS-NSM.

3.4. LCA-CTS-NSM characterization and optimization

3.4.1. Vesicle size and zeta potential assessments

The size and zeta potential of LCA-CTS-NSM dispersion were measured utilizing dynamic light scattering approach (Zetasizer Nano ZS, Malvern Instruments Ltd., USA) (Elkomy et al., 2021). Before

Table 1
The independent variable values, experimental runs, and measured response for LCA-CTS-NSM formulations.

Independent variables	Levels		
	(−1)	(0)	(1)
X_1: Span 60 (mg)	40	80	120
X_3: Chitosan concentration (*w/v* %)	0.1	0.25	0.4
X_2: Cholesterol (mg)	15	22.5	30

Run	Span 60 (mg)	Chitosan (w/v %)	Cholesterol (mg)	VS (nm)	ZP (mV)	EE (%)	CR (%)	PDI[¥]
1	80	0.25	22.5	175.3 ± 3.4	29.1 ± 1.5	53.2 ± 3.5	74.3 ± 5.6	0.25 ± 0.12
2	80	0.4	15	139.6 ± 2.5	38.1 ± 2.5	41.6 ± 4.1	83.5 ± 4.6	0.43 ± 0.15
3	120	0.25	30	280.4 ± 4.1	26.8 ± 2.1	67.3 ± 3.2	61.1 ± 5.2	0.32 ± 0.08
4	80	0.1	15	115.4 ± 1.6	22.7 ± 1.2	35.6 ± 2.2	84.3 ± 6.1	0.12 ± 0.06
5	120	0.25	15	135.2 ± 2.7	28.1 ± 2.6	42.8 ± 2.6	81.3 ± 2.4	0.36 ± 0.11
6	120	0.4	22.5	205.7 ± 3.6	35.6 ± 3.2	61.3 ± 3.2	69.2 ± 3.7	0.52 ± 0.16
7	120	0.1	22.5	161.4 ± 1.3	21.4 ± 1.8	59.3 ± 3.1	68.3 ± 4.3	0.24 ± 0.05
8	40	0.1	22.5	155.9 ± 2.4	24.2 ± 3.1	47.4 ± 2.7	79.3 ± 4.8	0.19 ± 0.03
9	40	0.25	30	256.7 ± 4.5	27.1 ± 2.5	55.6 ± 2.9	65.3 ± 3.2	0.38 ± 0.14
10	40	0.25	15	125.3 ± 2.8	26.2 ± 2.9	29.4 ± 3.2	86.6 ± 3.9	0.16 ± 0.02
11	80	0.1	30	257.3 ± 3.4	19.3 ± 0.9	63.4 ± 4.1	63.7 ± 3.2	0.42 ± 0.16
12	40	0.4	22.5	196.4 ± 4.2	37.2 ± 3.1	49.5 ± 2.8	76.2 ± 4.1	0.35 ± 0.09
13	80	0.4	30	301.5 ± 5.1	34.2 ± 2.4	65.4 ± 3.7	64.3 ± 5.3	0.18 ± 0.04
14	80	0.25	22.5	179.4 ± 2.6	31.5 ± 3.1	56.3 ± 2.5	72.6 ± 2.8	0.23 ± 0.03
15	80	0.25	22.5	184.3 ± 3.5	28.4 ± 2.3	52.6 ± 3.2	75.9 ± 3.2	0.14 ± 0.05
16	80	0.25	22.5	187.4 ± 2.2	31.3 ± 3.4	55.8 ± 4.2	71.4 ± 4.6	0.41 ± 0.13

[¥] not included in the optimization process.

analysis, 20 µL of formulated dispersions were diluted (1:10) with distilled water to eliminate the possibility of multi-scattering. The measurements were all made in triplicate at room temperature.

3.4.2. Entrapment efficiency measurement

The LCA-CTS-NSM nanovesicles were centrifuged via a cooling centrifuge (SIGMA 330 K, Germany) at 14,000 rpm (3 h, 4 °C) to separate the supernatant containing the unentrapped LCA (Elkomy et al., 2022d). The supernatant was diluted then the levels of LCA were estimated with the HPLC system. The precipitate containing LCA-loaded nanovesicles (entrapped LCA) was collected, reconstituted with phosphate buffer, and maintained at 4 °C for further characterization. LCA entrapment was calculated from the following formula (Eid et al., 2022; Elkomy et al., 2022c):

$$EE\% = \frac{(\text{LCA added (10 mg)} - \text{LCA in the supernatant})}{\text{LCA added (10 mg)}} \times 100$$

3.4.3. Measurement of cumulative release after 8 h (CR)

The Vertical Franz cells were used for the drug release experiments (2.5 cm^2 diffusion surface area). Before testing, a dialysis membrane was submerged for 24 h in a simulated nasal electrolyte solution (SNES) before being positioned between the donor and receptor chambers. Various LCA-CTS-NSM formulations containing 3 mg of LCA were introduced to the donor chamber. The receptor chamber was filled with 50 mL SNES, and the experiment was conducted at 37 °C with stirring at 50 rpm (Eid et al., 2019b). The aliquots were sampled after 8 h. Using the HPLC method, samples collected from the dissolution medium were analyzed, and the total amount of LCA released after 8 h was calculated.

3.4.4. Characterization of the optimal formula

3.4.4.1. Surface morphology. LCA-CTS-NSM morphology was analyzed by transmission electron microscopy (JEM-1400, Jeol, Tokyo, Japan) (Eid et al., 2022). For sample preparation, the optimized LCA-CTS-NSM dispersion was diluted, negatively stained with phosphotungstic acid (1% *w/v*) (Eid et al., 2019a; Elkomy et al., 2016), placed on a carbon-coated copper grid, and air-dried.

3.4.4.2. In vitro LCA release. The Vertical Franz cells were used for the drug release experiments (2.5 cm^2 diffusion surface area). Before testing, a dialysis membrane (MW cut off: 12000 Da) was submerged for 24 h in a simulated nasal electrolyte solution (SNES) before being positioned between the donor and receptor chambers. A certain quantity of optimized LCA-CTS-NSM and LCA-SOL with equivalent doses of LCA (3 mg) were introduced to the donor chamber. The receptor chamber was filled with 50 SNES, and the experiment was conducted at 37 °C with stirring at 50 rpm (Eid et al., 2019b). One mL was collected from the receptor chamber and replaced by one mL of fresh SNES at given time intervals (0.25, 0.5, 1, 2, 3, 4, 5, 6, 7, and 8 h). Using the HPLC method, samples collected from the dissolution medium were analyzed, and the levels of LCA were estimated. The cumulative percentage of medication released at specific intervals was plotted against time. The results from the release experiment were kinetically evaluated, and the mechanism of drug release from the various formulations was established. The correlation coefficient values (R^2) were calculated by employing zero- and first-order kinetics, the Higuchi model, the Hixson-Crowell model, and the Korsmeyer-Peppas model.

3.4.4.3. Ex vivo nasal diffusion of LCA. In a Franz Diffusion cell, an ex vivo nasal diffusion experiment was carried out using freshly dissected sheep nasal mucosa (2.5 cm^2). The sheep head was collected from a nearby butcher within 15 min following the sacrifice. After separating the nose from the head and thoroughly exposing the nasal septum, the nasal mucosa was removed using surgical scissors and forceps. The mucosal tissues were submerged for 30 min in a Phosphate Buffer with a pH of 6.5 (Abo El-Enin et al., 2022). The receptor chamber was filled with phosphate buffer (50 mL, pH 6.5), and the temperature was set at 37 °C to mimic body temperature (Eissa et al., 2022). The receptor vessel was stirred at 50 rpm. Then, with caution, freshly removed sheep nasal mucosa (0.2 mm thickness) was put between the donor and receptor vessels. 3 mL of optimized LCA-CTS-NSM and LCA-SOL, each corresponding to 1 mg/mL, on the nasal mucosal surface. One mL was collected from the receptor vessel at defined intervals and replaced with fresh medium. The HPLC system estimated the amount of LCA in the collected samples. Permeation parameters were computed, as stated previously (Elkomy et al., 2017).

3.5. Short-term stability

The stability of the optimized LCA-CTS-NSM dispersion was evaluated by storing it at 4 °C in sealed 20 mL glass vials (Elkomy et al., 2022d; Elkomy et al., 2023). At predetermined time intervals (0, 4, 8, and 12 weeks following formulation), the VS, EE, and ZP values of the stored formulations were examined (Elkomy et al., 2017). In addition, a visual inspection of the physical changes was conducted.

3.6. pH Assessments

The pH of LCA-CTS-NSM dispersion must be measured to guarantee that it does not irritate the nasal mucosa after intranasal delivery. The pH was estimated via the digital pH meter (Jenway, U.K).

3.7. In vivo studies

Male Wistar rats weighing 190–220 g and in good condition were utilized. The animals were given seven days to acclimate before the beginning of the study. All experiments were performed with the approval of the Beni-Suef University Institutional Animal Ethics Committee (Approval Serial No: 022–295) and following the Declaration of Helsinki.

3.8. Histopathological evaluation

Nasal toxicity was ruled out, and the safety of intranasal delivery of the LCA-CTS-NSM formulation was assessed using histological analysis (Eissa et al., 2022). The animals were split into three groups ($n = 3$). The negative control received 100 µL of normal saline, and the positive control groups received 1% sodium deoxycholate solution intranasally. The animals in the test group received 100 µL of the optimized LCA-CTS-NSM formulation in each nostril. After seven consecutive days of administration, the animals were sacrificed. The nasal epithelium was separated, decalcified, and preserved in buffered formalin (10% *v*/v) for subsequent staining with hematoxylin and eosin (H&E) and analysis with light microscopy (Abo El-Enin et al., 2022).

3.9. In vivo biodistribution analysis

The brain-targeting capabilities of LCA formulations delivered intravenously and intranasally were assessed by measuring drug distribution in the brain and systemic circulation at different time intervals. Animals were divided into three groups: group I received LCA-SOL (100 µL) intravenously (IV) via injection into the tail veins of the rats, group II and group III received LCA-SOL and the optimized LCA-CTS-NSM formulation intranasally (IN), respectively, via micropipette into both nostrils (50 µL in each nostril). Each group was subdivided into five subgroups according to time, and each subset had three rats that received 8 mg/kg of LCA. Inhaling enough diethyl ether to prevent sneezing during intranasal instillation rendered the rats sedated. Blood samples were collected from the retro-orbital vein and kept in heparinized tubes at predefined time points (0.5, 1, 2, 4, 8, and 12 h). The animals were euthanized through cervical dislocation immediately after blood collection, and their brains were dissected, washed with 0.9% sodium chloride, and cleared from any attached tissues or fluids (Eid et al., 2019b).

Centrifugation was used to separate the plasma from the acquired blood samples. Protein precipitation occurred when the plasma and acetonitrile were mixed (1:1). Following a 3-min vortex, the mixtures were centrifuged at 11000 rpm (25 min), and the supernatant was then stored at −21 °C until analysis with an HPLC system. Conversely, the brain was weighed, diluted with 0.9% NaCl, and homogenized. Brain homogenates were extracted with acetonitrile (1:1), vortexed for two minutes, centrifuged for 25 min (4000 rpm and 4 °C), and then the supernatant was stored at −21 °C until HPLC analysis.

3.10. Pharmacokinetic analysis

The Microsoft Excel add-on PK solver was used to compute the pharmacokinetic parameters in plasma and brain using a non-compartmental model (Elkomy et al., 2022a). The crucial pharmacokinetic variables, including peak plasma and brain concentrations (C_{max}), half-life ($t_{1/2}$), area under the curve ($AUC_{0\text{-}inf}$), the time required to achieve peak concentration (T_{max}), Drug targeting efficiency (DTE%), and Direct Transport to brain (DTP%) were calculated (Eid et al., 2019b). In addition, the brain bioavailability of LCA is calculated by the ratio of $AUC_{0\text{-}inf}$ in LCA-CTS-NSM (IN) versus LCA-SOL (IN) or LCA-SOL (IV).

3.11. Statistical analysis

Data are expressed as the mean ± SD. The *aov* function in the R program (version 4.2.0, 2022) was used to do an ANOVA test and display the significance of each variable. $P < 0.05$ was regarded as significant.

4. Results and discussion

4.1. Experiment design and optimization

The results of dependent variables (VS, EE, ZP, and CR) of sixteen experimental runs with various Span 60, cholesterol, and CTS levels are depicted in Table 1. Changes in Span 60, cholesterol, and CTS levels may substantially affect the surface modified NSM characteristics based on the broad range of dependent variable results. Table 2 depicts the mathematical equations that best reflect the relationship between the independent and dependent variables in terms of their coded values. The lack of fit was insignificant for all models, which indicates the adequacy of the models (Table 2). The adequate precision was evaluated to assess the model reliability in traversing the design space (Ahmad et al., 2015). Table 2 demonstrates that adequate precision was >4 and that the predicted R^2 values for all response variables were close to the adjusted R^2 values. In addition, the ANOVA analysis showed that cholesterol, Span 60, and CTS substantially impacted the response variables. Diagnostic model graphs confirming that the fitted models were adequate are shown in Fig. 1. As depicted in Table 1, polydispersity index (PDI) values of the developed LCA-CTS-NSM formulations ranged from 0.12 ± 0.06 to 0.52 ± 0.16, indicating that the prepared formulation had a narrow size distribution.

4.2. Model analysis of VS

For brain targeting, a VS between 100 and 300 nm was suggested, as previously stated (Abdelrahman et al., 2015; Olivier, 2005). The direct transfer of nanocarriers from the nasal mucosa to the brain could prevent or at least lessen opsonization to guarantee effective brain transport (Illum, 2015). VS assessment was conducted to illustrate the nanoscale range of the LCA-CTS-NSM formulations developed. As shown in Table 1, the VS of the produced LCA-CTS-NSM formulations varied between 115.4 and 301.5 nm. A reduced quadratic model was found suitable for VS values. Fig. 2 (A1&A2) illustrates the impact of Span 60, CTS, and cholesterol on LCA-CTS-NSM size.

Fig. 2 (A1&A2) shows that the VS increased when Span 60, cholesterol, and CTS levels rose. These results may be attributable to the low HLB of Span 60 (Eid et al., 2021). Similar results were reported (Bayindir and Yuksel, 2010; Fang et al., 2001). In addition, Span 60 has a low charge on its head group, which results in more aggregation (Liu and Guo, 2005). Due to the distinctive geometrical packing properties of cholesterol, it may align with the surfactant hydrocarbon chains. Moreover, cholesterol may give nanovesicles with a rigid structure and membrane-stabilizing properties. Consequently, high cholesterol levels increased VS (Fig. 1 A2) (Abdelkader et al., 2011; Attia et al., 2007).

Table 2
The analysis of response variables obtained by Design-Expert Software.

Source	VS		EE		ZP		CR	
	F	*p*	F	*p*	F	*p*	F	*p*
Model	290.17	< 0.0001	145.57	< 0.0001	40.09	< 0.0001	138.46	< 0.0001
X_1: Span 60	7.22	0.0211	102.10	< 0.0001	0.2795	0.6067	42.62	< 0.0001
X_2: Chitosan	72.38	< 0.0001	6.28	0.0292	117.86	< 0.0001	0.2698	0.6129
X_3: Cholesterol	1038.79	< 0.0001	448.68	< 0.0001	2.11	0.1716	372.50	< 0.0001
X_3^2	42.28	< 0.0001	25.22	0.0004				
Lack of Fit	1.58	0.3854	0.8009	0.6452	1.59	0.3853	0.4333	0.8549

Model	Reduced Quadratic	Reduced Quadratic	Linear	Linear
Adjusted R^2	0.9872	0.9747	0.8866	0.9649
R^2	0.9906	0.9815	0.9093	0.9719
%CV	3.33	3.27	6.50	1.01
Predicted R^2	0.9783	0.9600	0.8366	0.9526
Adequate precision	51.5296	39.5747	17.4094	36.5268
Standard deviation	6.37	1.71	1.87	0.0869

$$VS = 180.7 + 6.05.X_1 + 19.15.X_2 + 72.55.X_3 + 20.7.X_3^2$$
$$EE = 54.4 + 6.1.X_1 + 1.5.X_2 + 12.8.X_3 - 4.3.X_3^2$$
$$ZP = 28.8 - 0.35.X_1 + 7.19.X_2 - 0.96.X_3$$
$$\text{Sqrt}\,(CR) = 8.6 - 0.2.X_1 - 0.016.X_2 - 0.59.X_3$$

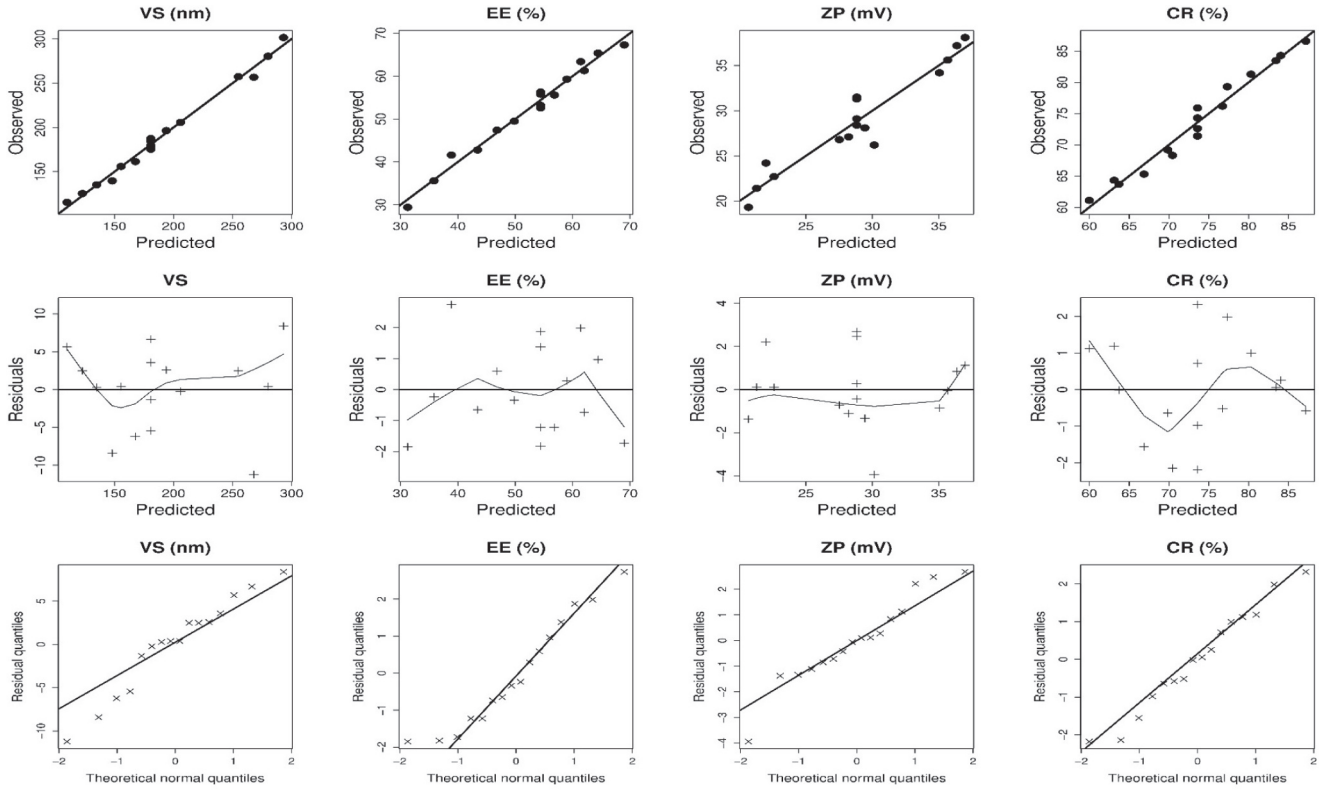

Fig. 1. Plots of model diagnostic information for LCA-CTS-NSM dependent variables.

Increasing CTS concentration slightly increased the NSM size (Fig. 1A1). This increase has resulted from the generation of a coating layer on the surface of the NSM. (For interpretation of the references to colour in this figure legend, the reader is referred to the web version of this article.)

4.3. Model analysis of EE

According to Table 1, entrapment ranged from 29.4% to 67.3% for the LCA-CTS-NSM formulations developed. The multi-factorial ANOVA indicated that the reduced quadratic model was suitable for entrapment results. Besides, entrapment was significantly impacted by all the independent factors (Span 60 amount, cholesterol amount, and CTS concentration).

As expected, increasing cholesterol increased drug entrapment (Fig. 1B2). Cholesterol has been extensively used as an additive agent in niosomal formation to confer membrane rigidity and to enhance

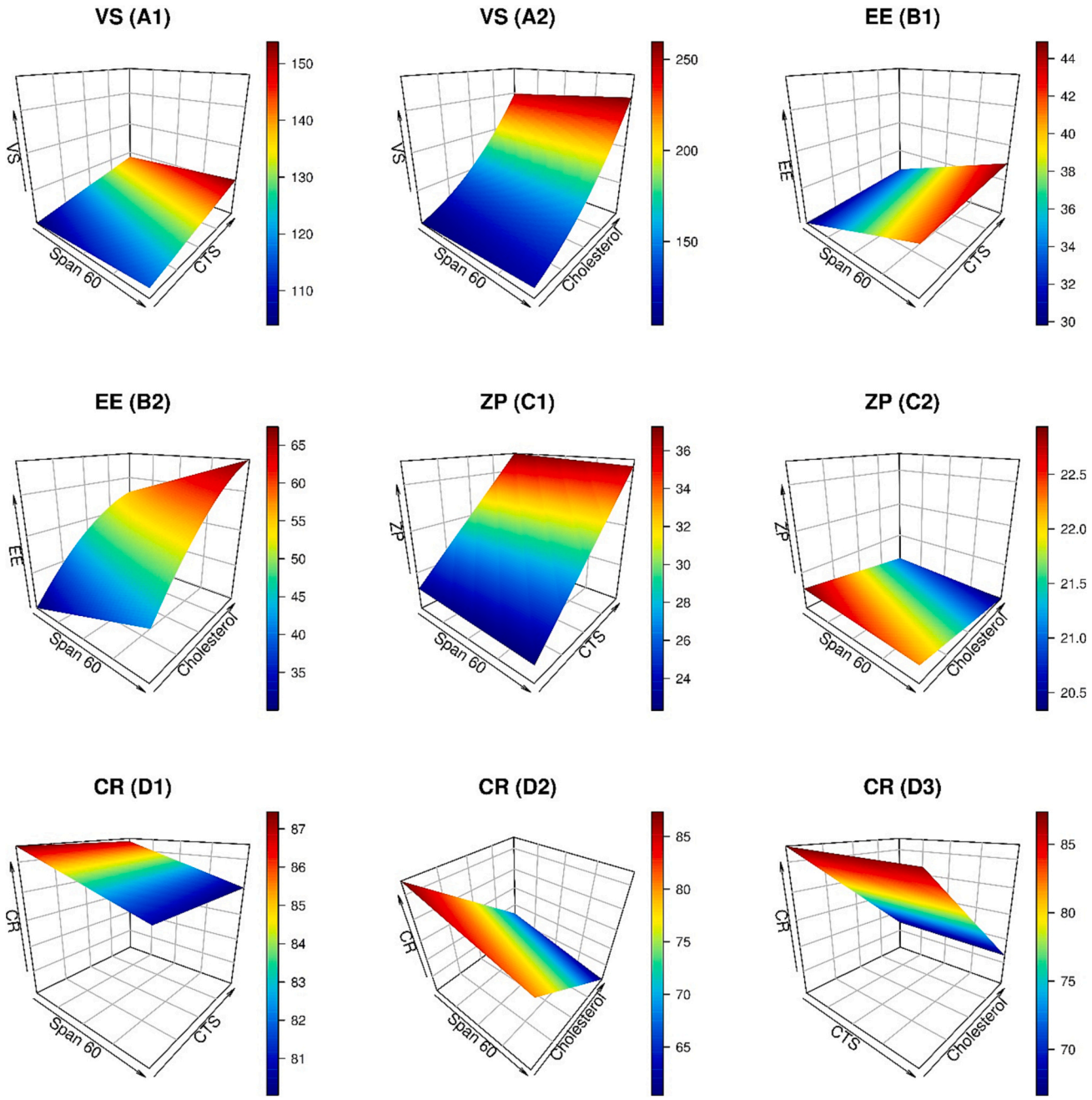

Fig. 2. 3D graphs demonstrating the effects of independent factors (Span 60, CTS, and Cholesterol) on LCA-CTS-NSM size (VS), entrapment (EE), zeta potential (ZP), and cumulative release (CR).

vesicular integrity and stability (Gugleva et al., 2019). Cholesterol has been observed to stabilize bilayers by modulating their cohesion and mechanical strength and hence it prevents leakage and slow permeation of solutes contained in the central aqueous cavity of the vesicles (Gugleva et al., 2019; Kumar and Rajeshwarrao, 2011). Consequently, presence of cholesterol is expected to limit LCA leakage from NSM vehicles. In addition, raising the level of CTS modestly reduced entrapment. These results are similar to previous outcomes (Eid et al., 2021). According to Figure 1 (B1&B2), high levels of Span 60 resulted in high entrapment. These findings may be attributed to the high phase transition temperature of Span 60, which allows for high encapsulation (Mokhtar et al., 2008). NSM created with Span 60 and cholesterol have a significantly better defined membrane with greater density, less leaky feature, and lower permeability (Pando et al., 2013).

4.4. Model analysis of ZP

Surface charge is a critical predictor of vesicle stability (Bayindir and Yuksel, 2010; Eid et al., 2021). ZP is a measure of the electrostatic repulsion between dispersed particles. Therefore, the dispersions with a high surface charge (absolute value) are expected to be stable and inhibit particle aggregation. Stable formulations generally have a ZP of more than +30 mV or less than −30 Mv (áO'Brien áO'Brien, 1990; Zubairu et al., 2015).

The ZP values in Table 1 ranged between 19.3 and 38.1 mV. These results indicated that the prepared formulation had high positive ZP, which promotes the interaction between positively charged LCA-CTS-NSM and the sialic groups (negatively charged) on the nasal mucosa (Elkomy et al., 2022b; Salade et al., 2018). In addition to boosting stability, the high positive charge induced by CTS can disrupt the tight

junctions between the epithelial cells efficiently, increasing the permeation of LCA across the nasal mucosa (Elkomy et al., 2022b).

It was determined that the linear model was suitable for assessing the ZP values. ANOVA Type III-Partial analysis revealed substantial effects for CTS levels, whereas cholesterol and Span 60 had no discernible effects on ZP.

As a result of the CTS amine group, the ZP of the LCA-CTS-NSM formulation was positively charged. Notably, the positive charge of the CTS amino group changed the surface charge from negative to positive, indicating that chitosan was effectively deposited onto the NSM surface (Eid et al., 2021). The ZP of 22.7 mV rose to 29.8 mV when CTS increased from 0.1 to 0.25%, as shown in Figure 1 (C1). The average magnitude of the ZP was increased to 36.9 mV when the CTS was increased to 0.4%. This was attributed to an increase in amino acid concentration, which added a positive charge to NSM, enhancing their stability in solution (Eid et al., 2022).

4.5. Model analysis of CR

According to Table 1, the CR after 8 h for the developed LCA-CTS-NSM formulations varied from 61.1% to 86.6%. The linear model was deemed suitable for CR analysis. Except for CTS, all the causative factors substantially affected CR. Span 60 and cholesterol had a negative effect on CR. High cholesterol levels considerably hinder the efflux of LCA from LCA-CTS-NSM, as seen in Figure 1 (D2&D3). This observation is in agreement with that reported in a previous study (Bekhet et al., 2022). Furthermore, high levels of Span 60 resulted in decreasing CR. These outcomes might be explained by the high level of Span 60 in the shell. The high transition temperature of the surfactant makes it more challenging for the medication to be released from vesicles(Abdelkader et al., 2014; Bekhet et al., 2022).

4.6. Formulation optimization

The Design expert® program made several recommendations that best fulfilled the specified constraints (minimum PS and maximum EE, ZP, and CR). The suggested formulation had a desirability value of 0.69 (Span 60: 120 mg, cholesterol: 18.6 mg, and CTS: 0.39%). The experimental, predicted, and prediction errors of dependable variables for the optimal formula are shown in Table 3. In addition, the calculated percentage of prediction error was <11% for all dependent variables. These results proved the validity of the final models. The Pareto chart illustrated the relatively standardized influences of formulation parameters on PS, EE, ZP, and CR (Fig. 3). Cholesterol levels had a more significant impact on VS, EE, and CR than Span 60 and CTS levels. However, the CTS level had the greatest effect on ZP.

4.7. Characterization of the optimal formula

4.7.1. Surface morphology

The TEM analysis indicated that LCA-CTS-NSM nanovesicles were spherical and distributed well without aggregations (Fig. 4). In addition, the CTS coating has no detrimental effect on niosomal nanovesicle architecture. Remarkably, the micrographs showed a thin layer covering the surface of nanovesicles, portraying a core-shell structure. The average VS was lower when TEM micrographs and Zetasizer data were compared. This might be due to the fact that TEM imaging was performed on dry materials (Motwani et al., 2008).

Table 3
The dependent variables values of experimental, predicted, and prediction error of the optimized formulation (LCA-CTS-NSM).

	VS (nm)	ZP (mV)	EE%	CR %
Experimental value	194.3	35.6	58.3	81.3
Predicted value	173.7	36.2	54.2	74.9
Prediction error (%) [£]	10.6	1.7	7.0	7.9

£Computed as (Experimental - Predicted) / Experimental x 100.

4.7.2. In vitro LCA release

LCA release patterns from LCA-CTS-NSM and LCA-SOL are illustrated in Fig. 5. After 2 h, LCA-SOL released 94.3% of the medication, but LCA-CTS-NSM released only 63.1%. The LCA-CTS-NSM release behavior demonstrated a short initial burst followed by an extended period over 8 h. This initial burst may have been caused by the discharge of LCA beneath or on the CTS coating. In contrast, the subsequent extended release resulted from the LCA being imprisoned inside the unique NSM structure. In contrast, LCA diffused swiftly from the solution into the receptor media in the case of LCA-SOL. The release data were subjected to a linear regression analysis, which showed that the optimized LCA-CTS-NSM and LCA-SOL released LCA according to first order kinetics.

4.7.3. Ex vivo permeation of LCA

The permeation properties of LCA-CTS-NSM and LCA-SOL are presented in Fig. 6. The ability of LCA-CTS-NSM and LCA-SOL to permeate the nasal membrane of sheep carrying a medication was compared. As shown in Fig. 6, the rate and extent of drug penetration in the case of LCA-CTS-NSM were much larger than in LCA-SOL. The nanoscale and the presence of CTS, which works as a penetration enhancer by opening a tight connection between epithelial cells, are responsible for these results (Eid et al., 2021). The mucoadhesive properties of CTS enable adherence to the surface of nasal mucosa for an extended time, hence boosting the amount of LCA that rapidly enters the nasal mucosa. As shown in Table 4, there was a substantial difference in flux (Jss) between LCA-CTS-NSM (41.9 ± 6.3 μg cm^{-2} h^{-1}) and LCA-SOL (24.5 ± 3.2 μg cm^{-2} h^{-1}). This is supported by the calculated permeability coefficient, which was almost twice greater for LCA-CTS-NSM than LCA-SOL for drug penetration via the nasal mucosa (Table 4).

4.7.4. Short-term stability

The optimized LCA-CTS-NSM exhibited excellent physical stability with no evidence of aggregation, separation, or drug precipitation during 12 weeks of storage at 4 °C. Fig. 7 illustrates the variations in VS, EE, and ZP of optimum LCA-CTS-NSM formulation over the storage period. Our statistical analysis showed a slight drop in ZP and EE and an increase in VS ($p > 0.05$). The minor rise in VS may be due to the modest swelling of CTS matrix (Abbas et al., 2022). This swelling may cause CTS matrix degradation, as shown by the reduction in ZP after 12 weeks (32.7 mV) compared to the starting point (35.6 mV). As a result of the entrapped LCA leakage, EE% dropped after 12 weeks (54.2%) compared to the initial EE% (58.3%). The results were consistent with those reported by Abbas et al. (Abbas et al., 2022).

4.7.5. Evaluation of pH

The healthy nasal mucosa pH range is 4.5 to 6.5, whereas the optimized LCA-CTS-NSM pH was 5.8. These results suggest that LCA-CTS-NSM is appropriate for intranasal administration.

4.7.6. Nasal histopathological studies

A critical criterion for accepting a formulation delivered through the nasal route is evaluating its potential for irritation and toxicity on the delicate nasal mucosa. This was assessed by providing saline (negative control), sodium deoxycholate (positive control), and the optimized LCA-CTS-NSM for one week. Fig. 8 depicts the nasal mucosa histology of all three groups. The cilia morphology was normal, and there was no inflammation or erosion in the saline-treated group (Fig. 8A). The sodium deoxycholate-treated positive control group exhibited substantial inflammation, epithelial hyperplasia, and submucosal infiltration of inflammatory cells (Fig. 8C). The group treated with LCA-CTS-NSM showed minimal nasal epithelial inflammation and infiltration of inflammatory cells (Fig. 8B). Overall, the findings indicate that the

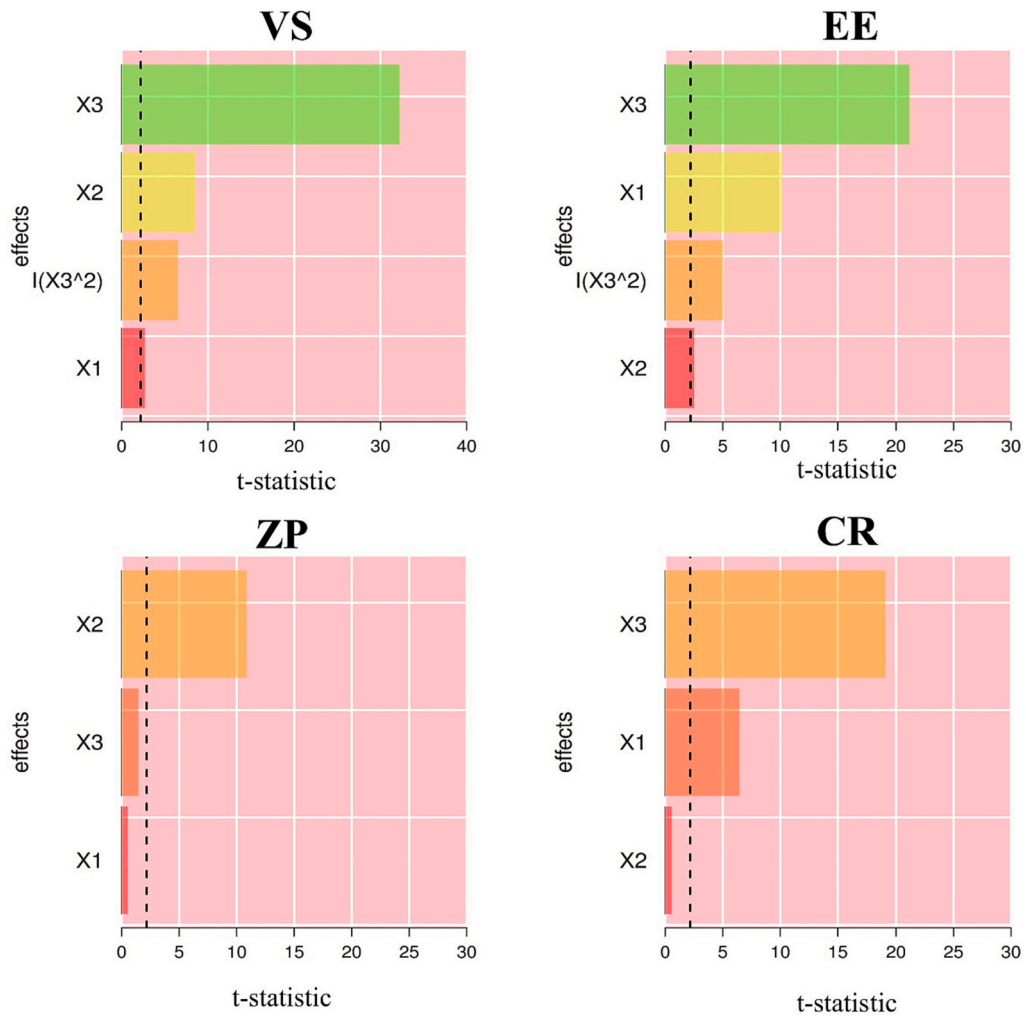

Fig. 3. The Pareto chart depicts the normalized effects of various variables (X_1: Span 60 amount, X_2: CTS concentration, and X_3: cholesterol amount).

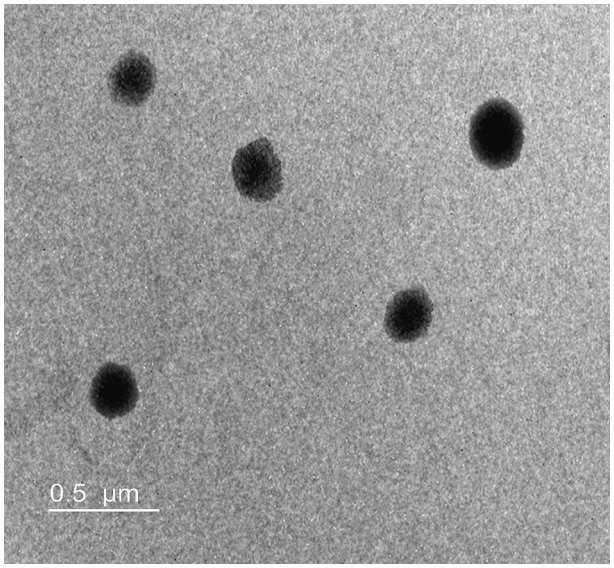

Fig. 4. Transmission electron micrograph **of** LCA-CTS-NSM dispersion.

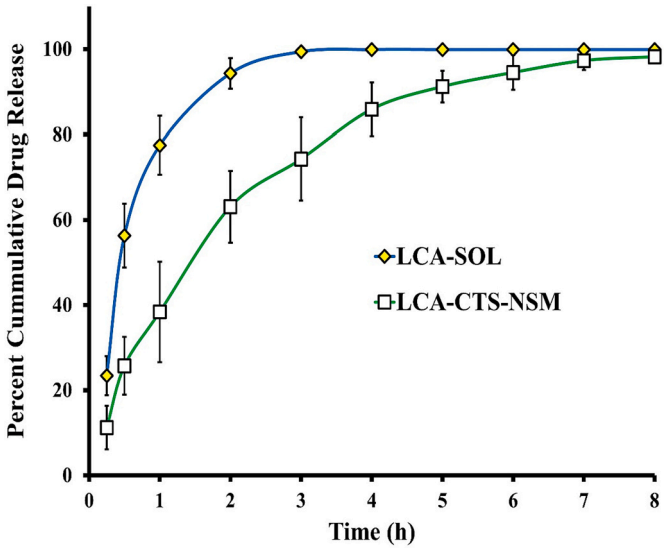

Fig. 5. The LCA release profiles from LCA-CTS-NSM and LCA-SOL.

proposed LCA-CTS-NSM formulation was safe and non-toxic to the nasal mucosa.

4.7.7. In vivo biodistribution analysis

After intranasal delivery of LCA-CTS-NSM and LCA-SOL and intravenous delivery of LCA-SOL, the pharmacokinetics of LCA in the brain

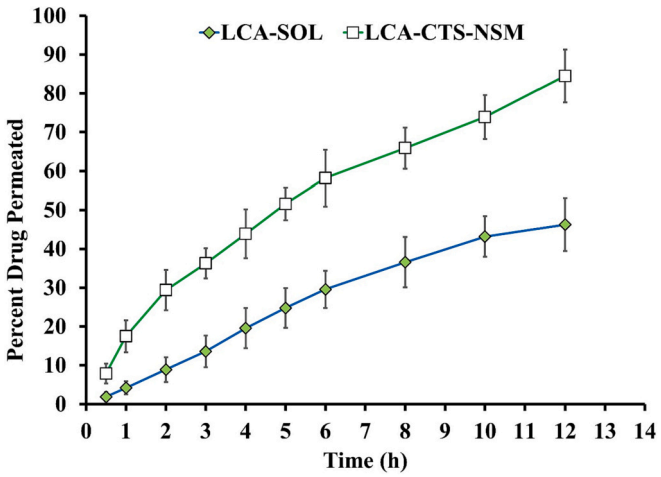

Fig. 6. The nasal diffusion profiles of LCA from LCA-SOL and LCA-CTS-NSM.

Table 4
The permeation parameters of LCA-CTS-NSM and LCA-SOL.

Formula	Flux (Jss) (μg cm^{-2} h^{-1})	Cumulative LCA permeated at 12 h (μg/cm^2)	Permeability coefficient (cm/h)
LCA-SOL	24.5 ± 3.2	555.6 ± 51.8	0.02449 ± 0.00023
LCA-CTS-NSM	41.9 ± 6.3	1014 ± 68.3	0.04189 ± 0.00016

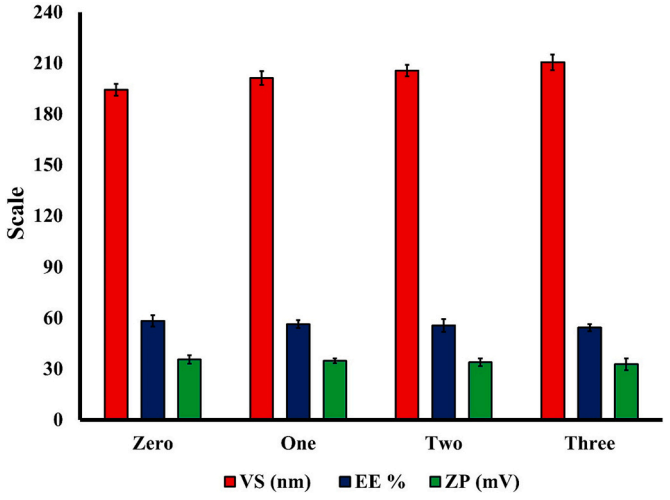

Fig. 7. The VS, ZP, and EE of the optimal formulation over 12 weeks of storage.

and plasma were examined. Figs. 9 and 10 demonstrate the levels of LCA in the brain and plasma, respectively. The pharmacokinetic characteristics of LCA-SOL (IV), LCA-CTS-NSM (IN), and LCA-SOL (IN) are listed in Table 5. As a result of the administration of LCA-CTS-NSM (IN) and LCA-SOL (IN), the plasma concentration of LCA reached its maximum after 1 h, according to pharmacokinetic data. Since intranasal delivery results in systemic drug absorption, it is anticipated that LCA will be present in plasma (Abo El-Enin et al., 2022; Eissa et al., 2022). After 0.5 h of IV administration, on the other hand, the plasma levels reached their highest point and then dropped quickly over the next 2 h. The maximum level of LCA in the brain occurred after 0.5, 1, and 1 h of administration of LCA-SOL (IV), LCA-SOL (IN), and LCA-CTS-NSM (IN), respectively. The plasma C_{max} of LCA-CTS-NSM was 1335 ± 317 ng/mL, LCA-SOL (IN) was 843 ± 184 ng/mL, and LCA-SOL (IV) was 4490 ± 412 ng/mL. The brain C_{max} of LCA-CTS-NSM was 1639 ± 319 ng/mL, LCA-SOL (IN) was 628 ± 128 ng/mL, and LCA-SOL (IV) was 1254 ± 294 ng/mL. As displayed in Table 5, intravenous administration of LCA-SOL resulted in significantly higher Cmax and $AUC_{0\text{-inf}}$ values compared to intranasal formulations, which may be attributed to increased LCA transport across the BBB via passive diffusion as a result of the initial increase in plasma LCA concentration following IV administration (Khallaf et al., 2020).

C_{max} in the brain and plasma was higher for LCA-CTS-NSM (IN) than for LCA-SOL (IN). In addition, LCA-CTS-NSM greatly improves LCA bioavailability, as seen by the high $AUC_{0\text{-inf}}$ values (Table 5). LCA-CTS-NSM demonstrated a brain bioavailability 7 times higher than LCA-SOL (IN). In addition, the LCA-CTS-NSM demonstrated a brain bioavailability 4.5 times higher than the LCA-SOL (IV). These findings are consistent with the ex vivo permeation data that revealed that the rate and extent of drug penetration in the case of LCA-CTS-NSM were much larger than in LCA-SOL. Besides, these results might help to explain how the nasal formulation is delivered directly from the nose to the brain, circumventing the BBB.

Table 5 displays the estimated brain-to-blood ratios for AUC0-inf for comparison and brain targeting evaluation. LCA-CTS-NSM (IN) brain-to-blood ratios were higher when compared to LCA-SOL (IV) and LCA-SOL (IN). The LCA-CTS-NSM (IN) exhibited a much longer elimination half-life and lower elimination rate constant (Ke) than LCA-SOL (IN) and LCA-SOL (IV). These results can be attributed to two issues. First, the comparatively slow release of LCA from the LCA-CTS-NSM reservoir leads to slowed elimination and distribution compared to LCA release from LCA-SOL (IV) and LCA-SOL (IN). Second, the small size of LCA-CTS-NSM, as it has been reported that nanoparticles bypass liver and spleen filtration, have long blood circulation, and escape the RES (Gastaldi et al., 2014). Additionally, the CTS coating provided a positive charge and a steric hindrance effect that decreased opsonin's ability to bind to NSM nanovesicles in plasma, limiting RES absorption and prolonging retention duration (Salem et al., 2020).

The DTP and DTE determine the amount of drug entering the brain via the olfactory pathway. The LCA-CTS-NSM (IN) exhibited the highest DTE and DTP, with values of 694% and 86%, respectively, indicating that the surface-modified niosomes enhanced LCA brain targeting in comparison to LCA-SOL.

As far as we know, only one study reported an attempt to deliver LCA to the brain through the intranasal pathway (Gonçalves et al., 2021). This study administered LCA intranasally in the form of *an* in-situ gel system to augment LCA brain bioavailability. Overall, the concentration–time profiles of LCA administered intravenously and intranasally were equivalent, indicating comparable pharmacological effects. However, after IN instillation, brain drug exposure increased, suggesting direct transport from the nasal cavity to the brain, with a DTE of 128.67% and a DTP of 22.28%. Additionally, both administration routes had identical t_{max} in the brain, underlining the possibility of IN delivery for treating acute convulsive cases. Additionally, the MRT value of LCA in the brain supports the sustained concentrations and efficacy of IN administration during long-term LCA therapy.

Furthermore, the CTS-coated NSM was extensively utilized to boost the brain bioavailability of several drugs such as pentamidine (Rinaldi et al., 2018), methotrexate (Ourani-Pourdashti et al., 2022), clonazepam (Nerli et al., 2023), olanzapine (Khallaf et al., 2020), curcumin (Salehi et al., 2022). The ability of NSM to circumvent nasal route limitations like ciliary clearance as well as other benefits like being inexpensive, stable, biodegradable, and simple to prepare, have made them promising nanocarriers when considering the delivery of drugs to the brain through the nasal route (Khallaf et al., 2020; Moghassemi and Hadjizadeh, 2014). Interestingly, CTS is a natural polymer that can improve the mucoadhesive properties of NSM (Eid et al., 2021). When NSM are coated with CTS, they can adhere to the nasal mucosa, allowing for prolonged contact and enhanced drug transport to the brain (Khallaf et al., 2020). In addition, the coating of NSM with CTS improves the drug

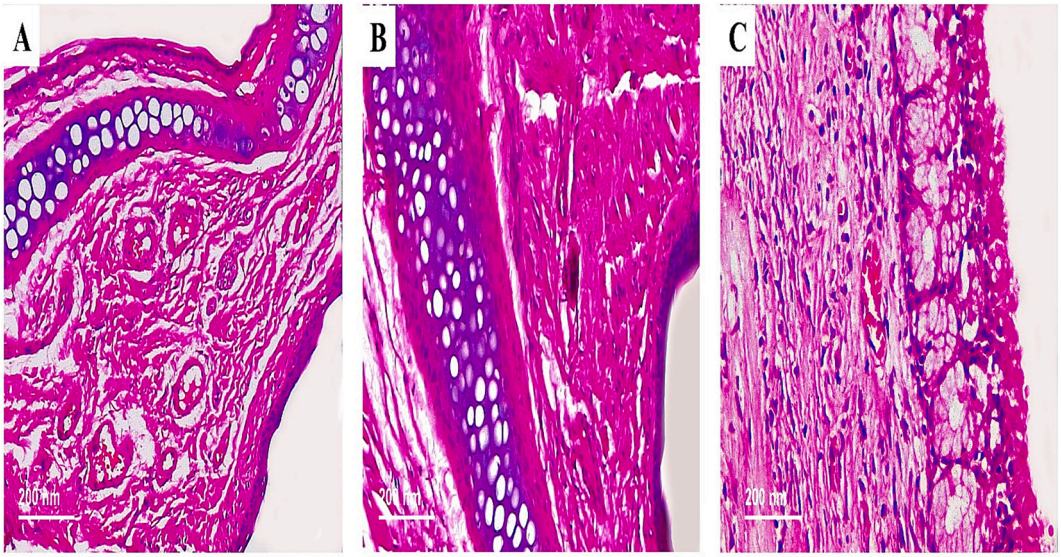

Fig. 8. Light photomicrographs showing nasal epithelium of (A) the control group; (B) the LCA-CTS-NSM group; and (C) the positive group. H&E stain X200.

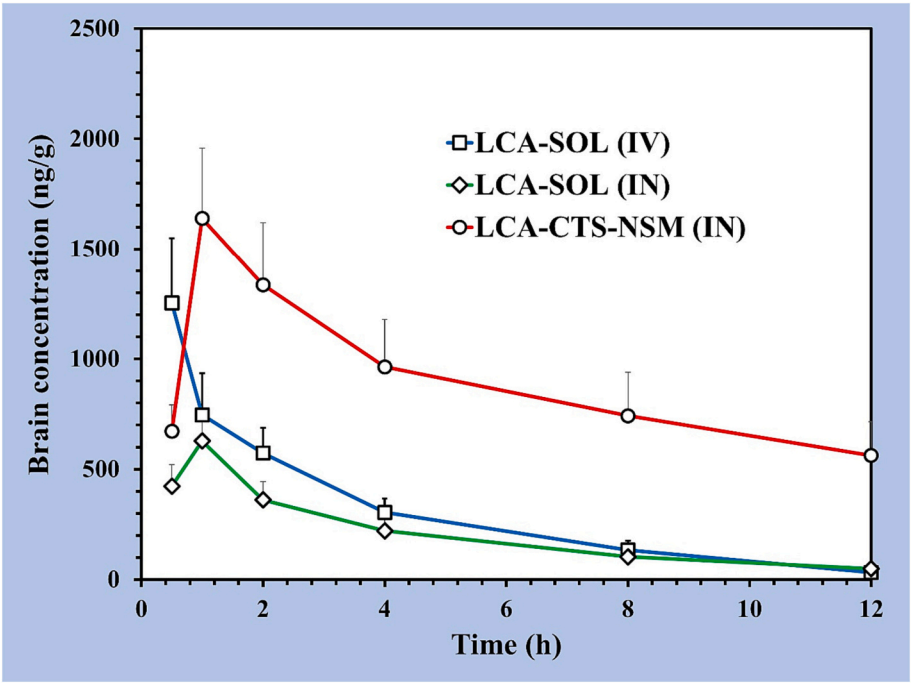

Fig. 9. Lacosamide concentrations in rat brain after intranasal administration of LCA-SOL and LCA-CTS-NSM and intravenous administration of LCA-SOL.

stability of NSM, protecting the encapsulated drug from degradation and maintaining its therapeutic efficacy (Elkomy et al., 2022b; Miatmoko et al., 2021). In addition, it has been reported that CTS can facilitate penetration by loosening the tight junction between epithelial cells (Elkomy et al., 2022b).

Collectively, these findings are attributable to the penetrating impact of the formulated LCA-CTS-NSM and the improved LCA transcellular transport by non-ionic surfactants (Khallaf et al., 2020). Additionally, the surface coating with CTS offers several advantages, including tight-junctional modulation, extended retention duration in the nasal cavity, extensive mucoadhesive characteristics, and augmented permeation potential by boosting the paracellular transport mechanism (Abo El-Enin et al., 2022; Eid et al., 2021; Elkomy et al., 2022b).

5. Conclusions

In the current work, a safe, optimal LCA-CTS-NSM formulation was created to increase residence duration on the nasal mucosa, physical stability, and bioavailability of LCA in brain tissues. Compared to the LCA solution, LCA-CTS-NSM demonstrated a delayed release profile, a 2-fold increase in nasal diffusion, increased bioavailability, and improved brain distribution after intranasal administration. Current research indicates that LCA-CTS-NSM nasal drops have the potential to be developed as a nanoplatform technology for partial-onset seizure management.

Funding

This work was funded by the Deanship of Scientific Research at Jouf

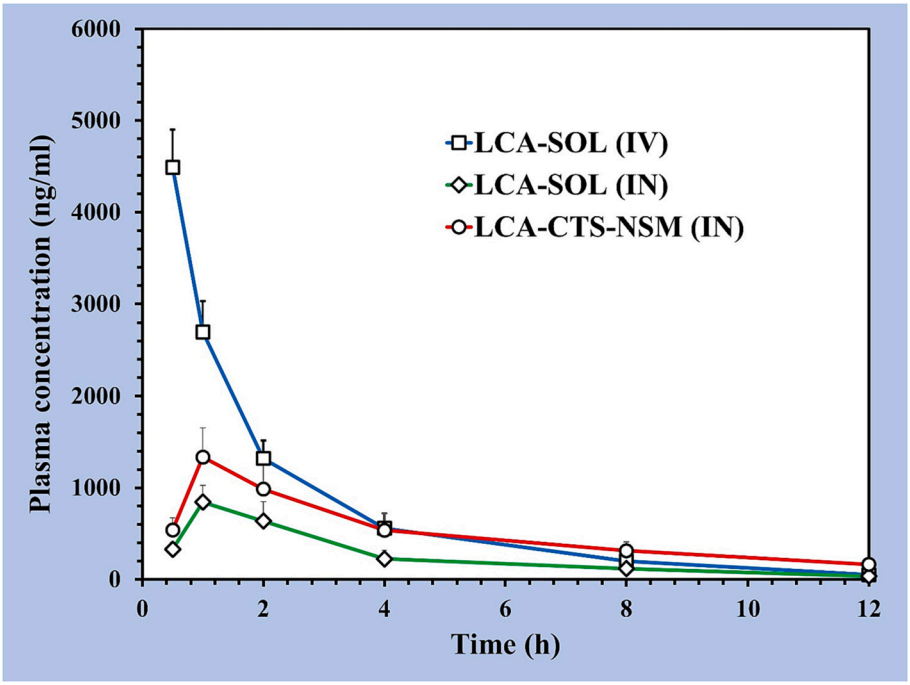

Fig. 10. Lacosamide concentrations in rat plasma after intranasal administration of LCA-SOL and LCA-CTS-NSM and intravenous administration of LCA-SOL.

Table 5
Pharmacokinetic parameters of LCA-CTS-NSM (IN), LCA-SOL (IN), and LCA-SOL (IV).

Formula	Tissue	Ke (h^{-1})	$t_{1/2}$ (h)	T_{max} (h)	C_{max} (ng/mL)	$AUC_{0\text{-}inf}$ (ng/mL*h)	DTP	DTE	AUC_{brain}/AUC_{blood}
LCA-SOL (IV)	Brain	0.278	2.5	0.5	1254	4200	–	–	0.39
	Plasma	0.317	2.19	0.5	4490	10,848			
LCA-SOL (IN)	Brain	0.188	3.68	1	628	2657	54.9	221.8	0.86
	Plasma	0.28	2.47	1	843	3094			
LCA-CTS-NSM (IN)	Brain	0.067	10.28	1	1639	18,885	85.6	693.9	2.69
	Plasma	0.149	4.65	1	1335	7029			

University under grant No. (DSR-2021-01-03125).

Institutional review board statement

The animal study protocol was approved by the Beni-Suef University Institutional Animal Ethics Committee (Approval Serial No: 022-295).

CRediT authorship contribution statement

Alaa S. Tulbah: Methodology, Writing – review & editing, Funding acquisition, Validation. **Mohammed H. Elkomy:** Conceptualization, Methodology, Writing – review & editing, Supervision, Funding acquisition. **Randa Mohammed Zaki:** Methodology, Resources, Writing – review & editing. **Hussein M. Eid:** Conceptualization, Formal analysis, Methodology, Writing – original draft, Investigation, Writing – review & editing. **Essam M. Eissa:** Methodology, Validation, Resources. **Adel A. Ali:** Methodology, Validation, Resources. **Heba A. Yassin:** Methodology, Validation, Resources. **Basmah Nasser Aldosari:** Methodology, Validation, Funding acquisition. **Ibrahim A. Naguib:** Methodology, Validation. **Amira H. Hassan:** Methodology, Validation, Resources.

Declaration of Competing Interest

The authors wish to declare no interest is involved in this publication.

Data availability

Data is contained within the article.

Acknowledgment

This work was funded by the Deanship of Scientific Research at Jouf University under grant No. (DSR-2021-01-03125).

References

Abbas, H., El Sayed, N.S., Youssef, N.A.H.A., ME Gaafar, P., Mousa, M.R., Fayez, A.M., Elsheikh, M.A., 2022. Novel luteolin-loaded chitosan decorated nanoparticles for brain-targeting delivery in a sporadic Alzheimer's disease mouse model: focus on antioxidant, anti-inflammatory, and amyloidogenic pathways. Pharmaceutics 14, 1003.

Abdelkader, H., Ismail, S., Kamal, A., Alany, R.G., 2011. Design and evaluation of controlled-release niosomes and discomes for naltrexone hydrochloride ocular delivery. J. Pharmaceut. Sci. 100, 1833–1846.

Abdelkader, H., Farghaly, U., Moharram, H., 2014. Effects of surfactant type and cholesterol level on niosomes physical properties and in vivo ocular performance using timolol maleate as a model drug. J. Pharmaceut. Investigat. 44, 329–337.

Abdelrahman, F.E., Elsayed, I., Gad, M.K., Badr, A., Mohamed, M.I., 2015. Investigating the cubosomal ability for transnasal brain targeting: in vitro optimization, ex vivo permeation and in vivo biodistribution. Int. J. Pharmaceut. 490, 281–291.

Abo El-Enin, H.A., Elkomy, M.H., Naguib, I.A., Ahmed, M.F., Alsaidan, O.A., Alsalahat, I., Ghoneim, M.M., Eid, H.M., 2022. Lipid nanocarriers overlaid with chitosan for brain delivery of berberine via the nasal route. Pharmaceuticals 15, 281.

Ahmad, A., Alkharfy, K.M., Wani, T.A., Raish, M., 2015. Application of Box–Behnken design for ultrasonic-assisted extraction of polysaccharides from Paeonia emodi. Int. J. Biol. Macromol. 72, 990–997.

Al-Massri, K.F., Ahmed, L.A., El-Abhar, H.S., 2018. Pregabalin and lacosamide ameliorate paclitaxel-induced peripheral neuropathy via inhibition of JAK/STAT signaling pathway and Notch-1 receptor. Neurochem. Int. 120, 164–171.
Amengual-Gual, M., Ulate-Campos, A., Loddenkemper, T., 2019. Status epilepticus prevention, ambulatory monitoring, early seizure detection and prediction in at-risk patients. Seizure 68, 31–37.
áO'Brien, R.W., 1990. Electroacoustic studies of moderately concentrated colloidal suspensions. Faraday Discuss. Chem. Soc. 90, 301–312.
Attia, I.A., El-Gizawy, S.A., Fouda, M.A., Donia, A.M., 2007. Influence of a niosomal formulation on the oral bioavailability of acyclovir in rabbits. AAPS PharmSciTech 8, 206–212.
Bayindir, Z.S., Yuksel, N., 2010. Characterization of niosomes prepared with various nonionic surfactants for paclitaxel oral delivery. J. Pharmaceut. Sci. 99, 2049–2060.
Bekhet, M.A., Ali, A.A., Kharshoum, R.M., El-Ela, F.I.A., Salem, H.F., 2022. Intranasal niosomal in situ gel as a novel strategy for improving citicoline efficacy and brain delivery in treatment of epilepsy. In: Vitro and Ex Vivo Characterization and in Vivo Pharmacodynamics Investigation. Journal of Pharmaceutical Sciences.
Carmland, M.E., Kreutzfeldt, M., Holbech, J.V., Andersen, N.T., Jensen, T.S., Bach, F.W., Sindrup, S.H., Finnerup, N.B., 2019. Effect of lacosamide in peripheral neuropathic pain: study protocol for a randomized, placebo-controlled, phenotype-stratified trial. Trials 20, 1–8.
Costa, C., Moreira, J., Amaral, M., Lobo, J.S., Silva, A.C., 2019. Nose-to-brain delivery of lipid-based nanosystems for epileptic seizures and anxiety crisis. J. Control. Release 295, 187–200.
de Biase, S., Gigli, G.L., Valente, M., Merlino, G., 2014. Lacosamide for the treatment of epilepsy. Expert Opin. Drug Metab. Toxicol. 10, 459–468.
Eid, H.M., Elkomy, M.H., El Menshawe, S.F., Salem, H.F., 2019a. Development, optimization, and in vitro/in vivo characterization of enhanced lipid nanoparticles for ocular delivery of ofloxacin: the influence of pegylation and chitosan coating. AAPS PharmSciTech 20, 1–14.
Eid, H.M., Elkomy, M.H., El Menshawe, S.F., Salem, H.F., 2019b. Transfersomal nanovesicles for nose-to-brain delivery of ofloxacin for better management of bacterial meningitis: Formulation, optimization by Box-Behnken design, characterization and in vivo pharmacokinetic study. J. Drug Deliv. Sci. Technol. 54, 101304.
Eid, H.M., Naguib, I.A., Alsantali, R.I., Alsalahat, I., Hegazy, A.M., 2021. Novel chitosan-coated niosomal formulation for improved management of bacterial conjunctivitis: a highly permeable and efficient ocular nanocarrier for azithromycin. J. Pharmaceut. Sci. 110, 3027–3036.
Eid, H.M., Ali, A.A., Ali, A.M.A., Eissa, E.M., Hassan, R.M., El-Ela, F.I.A., Hassan, A.H., 2022. Potential use of tailored citicoline chitosan-coated liposomes for effective wound healing in diabetic rat model. Int. J. Nanomedicine 17, 555.
Eissa, E.M., Elkomy, M.H., Eid, H.M., Ali, A.A., Abourehab, M.A., Alsubaiyel, A.M., Naguib, I.A., Alsalahat, I., Hassan, A.H., 2022. Intranasal delivery of granisetron to the brain via nanostructured cubosomes-based in situ gel for improved management of chemotherapy-induced emesis. Pharmaceutics 14, 1374.
Elkomy, M.H., Elmenshawe, S.F., Eid, H.M., Ali, A.M., 2016. Topical ketoprofen nanogel: artificial neural network optimization, clustered bootstrap validation, and in vivo activity evaluation based on longitudinal dose response modeling. Drug Deliv. 23, 3294–3306.
Elkomy, M.H., El Menshawe, S.F., Eid, H.M., Ali, A.M., 2017. Development of a nanogel formulation for transdermal delivery of tenoxicam: a pharmacokinetic–pharmacodynamic modeling approach for quantitative prediction of skin absorption. Drug Dev. Ind. Pharm. 43, 531–544.
Elkomy, M.H., Elmowafy, M., Shalaby, K., Azmy, A.F., Ahmad, N., Zafar, A., Eid, H.M., 2021. Development and machine-learning optimization of mucoadhesive nanostructured lipid carriers loaded with fluconazole for treatment of oral candidiasis. Drug Dev. Ind. Pharm. 47, 246–258.
Elkomy, M.H., Abou-Taleb, H.A., Eid, H.M., Yassin, H.A., 2022a. Fabrication and in vitro/in vivo appraisal of metronidazole intra-gastric buoyant sustained-release tablets in healthy volunteers. Pharmaceutics 14, 863.
Elkomy, M.H., Ali, A.A., Eid, H.M., 2022b. Chitosan on the surface of nanoparticles for enhanced drug delivery: a comprehensive review. J. Control. Release 351, 923–940.
Elkomy, M.H., Alruwaili, N.K., Elmowafy, M., Shalaby, K., Zafar, A., Ahmad, N., Alsalahat, I., Ghoneim, M.M., Eissa, E.M., Eid, H.M., 2022c. Surface-modified bilosomes nanogel bearing a natural plant alkaloid for safe management of rheumatoid arthritis inflammation. Pharmaceutics 14, 563.
Elkomy, M.H., Eid, H.M., Elmowafy, M., Shalaby, K., Zafar, A., Abdelgawad, M.A., Rateb, M.E., Ali, M.R., Alsalahat, I., Abou-Taleb, H.A., 2022d. Bilosomes as a promising nanoplatform for oral delivery of an alkaloid nutraceutical: improved pharmacokinetic profile and snowballed hypoglycemic effect in diabetic rats. Drug Deliv. 29, 2694–2704.
Elkomy, M.H., Zaki, R.M., Alsaidan, O.A., Elmowafy, M., Zafar, A., Shalaby, K., Abdelgawad, M.A., Abo El-Ela, F.I., Rateb, M.E., Naguib, I.A., 2023. Intranasal nanotransferosomal gel for quercetin brain targeting: I. Optimization, characterization, brain localization, and cytotoxic studies. Pharmaceutics 15, 1805.
Elsenosy, F.M., Abdelbary, G.A., Elshafeey, A.H., Elsayed, I., Fares, A.R.J.I.J.o.N, 2020. Brain Targeting of Duloxetine HCL via Intranasal Delivery of Loaded Cubosomal Gel: In vitro Characterization, ex vivo Permeation, and in vivo Biodistribution Studies, 15, p. 9517.
Engel Jr., J., Pitkänen, A., 2020. Biomarkers for epileptogenesis and its treatment. Neuropharmacology 167, 107735.
Fang, J.-Y., Yu, S.-Y., Wu, P.-C., Huang, Y.-B., Tsai, Y.-H., 2001. In vitro skin permeation of estradiol from various proniosome formulations. Int. J. Pharmaceut. 215, 91–99.
Gangurde, P.K., Ajitkumar, B.N., Kumar, L., 2019. Lamotrigine lipid nanoparticles for effective treatment of epilepsy: a focus on brain targeting via nasal route. J. Pharmaceut. Innov. 14, 91–111.
Gastaldi, L., Battaglia, L., Peira, E., Chirio, D., Muntoni, E., Solazzi, I., Gallarate, M., Dosio, F., 2014. Solid lipid nanoparticles as vehicles of drugs to the brain: current state of the art. Eur. J. Pharmaceut. Biopharm. 87, 433–444.
Gonçalves, J., Alves, G., Fonseca, C., Carona, A., Bicker, J., Falcão, A., Fortuna, A., 2021. Is intranasal administration an opportunity for direct brain delivery of lacosamide? Eur. J. Pharmaceut. Sci. 157, 105632.
Gugleva, V., Titeva, S., Rangelov, S., Momekova, D., 2019. Design and in vitro evaluation of doxycycline hyclate niosomes as a potential ocular delivery system. Int. J. Pharmaceut. 567, 118431.
Halford, J.J., Lapointe, M., 2009. Clinical perspectives on lacosamide. Epilepsy Curr. 9, 1–9.
Illum, L., 2015. Intranasal delivery to the central nervous system. Blood-Brain Barrier Drug Disc. 535–565.
Kazi, K.M., Mandal, A.S., Biswas, N., Guha, A., Chatterjee, S., Behera, M., Kuotsu, K., 2010. Niosome: a future of targeted drug delivery systems. J. Adv. Pharmaceut. Technol. Res. 1, 374.
Khallaf, R.A., Aboud, H.M., Sayed, O.M., 2020. Surface modified niosomes of olanzapine for brain targeting via nasal route; preparation, optimization, and in vivo evaluation. J. Liposome Res. 30, 163–173.
Kim, G.-H., Byeon, J.H., Eun, B.-L., 2017. Neuroprotective effect of lacosamide on hypoxic-ischemic brain injury in neonatal rats. J. Clin. Neurol. 13, 138–143.
Kumar, G.P., Rajeshwarrao, P., 2011. Nonionic surfactant vesicular systems for effective drug delivery—an overview. Acta Pharmaceut. Sin. B 1, 208–219.
Lazarowski, A., Czornyj, L., Lubieniecki, F., Girardi, E., Vazquez, S., D'Giano, C., 2007. ABC transporters during epilepsy and mechanisms underlying multidrug resistance in refractory epilepsy. Epilepsia 48, 140–149.
Lionetto, L., Negro, A., Palmisani, S., Gentile, G., Fiore, M.R.D., Mercieri, M., Simmaco, M., Smith, T., Al-Kaisy, A., Arcioni, R., 2012. Emerging treatment for chronic migraine and refractory chronic migraine. Exp. Opin. Emerg. Drugs 17, 393–406.
Liu, T., Guo, R., 2005. Preparation of a highly stable niosome and its hydrotrope-solubilization action to drugs. Langmuir 21, 11034–11039.
Miatmoko, A., Safitri, S.A., Aquila, F., Cahyani, D.M., Hariawan, B.S., Hendrianto, E., Hendradi, E., Sari, R., 2021. Characterization and distribution of niosomes containing ursolic acid coated with chitosan layer. Res. Pharmaceut. Sci. 16, 660.
Moghassemi, S., Hadjizadeh, A., 2014. Nano-niosomes as nanoscale drug delivery systems: an illustrated review. J. Control. Release 185, 22–36.
Mokhtar, M., Sammour, O.A., Hammad, M.A., Megrab, N.A., 2008. Effect of some formulation parameters on flurbiprofen encapsulation and release rates of niosomes prepared from proniosomes. Int. J. Pharmaceut. 361, 104–111.
Motwani, S.K., Chopra, S., Talegaonkar, S., Kohli, K., Ahmad, F.J., Khar, R.K., 2008. Chitosan–sodium alginate nanoparticles as submicroscopic reservoirs for ocular delivery: Formulation, optimisation and in vitro characterisation. Eur. J. Pharmaceut. Biopharm. 68, 513–525.
Moutal, A., Chew, L.A., Yang, X., Wang, Y., Yeon, S.K., Telemi, E., Meroueh, S., Park, K. D., Shrinivasan, R., Gilbraith, K.B., 2016. (S)-lacosamide inhibition of CRMP2 phosphorylation reduces postoperative and neuropathic pain behaviors through distinct classes of sensory neurons identified by constellation pharmacology. Pain 157, 1448.
Musumeci, T., Serapide, M.F., Pellitteri, R., Dalpiaz, A., Ferraro, L., Dal Magro, R., Bonaccorso, A., Carbone, C., Veiga, F., Sancini, G., 2018. Oxcarbazepine free or loaded PLGA nanoparticles as effective intranasal approach to control epileptic seizures in rodents. Eur. J. Pharmaceut. Biopharm. 133, 309–320.
Musumeci, T., Bonaccorso, A., Puglisi, G., 2019. Epilepsy disease and nose-to-brain delivery of polymeric nanoparticles: an overview. Pharmaceutics 11, 118.
Nerli, G., Robla, S., Bartalesi, M., Luceri, C., D'Ambrosio, M., Csaba, N., Maestrelli, F., 2023. Chitosan coated niosomes for nose-to-brain delivery of clonazepam: formulation, stability and permeability studies. Carbohydrate Polym. Technol. Appl. 100332.
Olivier, J.-C., 2005. Drug transport to brain with targeted nanoparticles. NeuroRx 2, 108–119.
Organization, W.H, 2019. Epilepsy: A Public Health Imperative. World Health Organization.
Ourani-Pourdashti, S., Mirzaei, E., Heidari, R., Ashrafi, H., Azadi, A., 2022. Preparation and evaluation of niosomal chitosan-based in situ gel formulation for direct nose-to-brain methotrexate delivery. Int. J. Biol. Macromol. 213, 1115–1126.
Panda, D.S., Eid, H.M., Elkomy, M.H., Khames, A., Hassan, R.M., Abo El-Ela, F.I., Yassin, H.A., 2021. Berberine encapsulated lecithin–chitosan nanoparticles as innovative wound healing agent in type II diabetes. Pharmaceutics 13, 1197.
Pando, D., Gutiérrez, G., Coca, J., Pazos, C., 2013. Preparation and characterization of niosomes containing resveratrol. J. Food Eng. 117, 227–234.
Pires, P.C., Santos, L.T., Rodrigues, M., Alves, G., Santos, A.O., 2021. Intranasal fosphenytoin: the promise of phosphate esters in nose-to-brain delivery of poorly soluble drugs. Int. J. Pharmaceut. 592, 120040.
Rinaldi, F., Hanieh, P.N., Chan, L.K.N., Angeloni, L., Passeri, D., Rossi, M., Wang, J.T.-W., Imbriano, A., Carafa, M., Marianecci, C., 2018. Chitosan glutamate-coated niosomes: a proposal for nose-to-brain delivery. Pharmaceutics 10, 38.
Rizzo, A., Donzelli, S., Girgenti, V., Sacconi, A., Vasco, C., Salmaggi, A., Blandino, G., Maschio, M., Ciusani, E., 2017. In vitro antineoplastic effects of brivaracetam and lacosamide on human glioma cells. J. Exp. Clin. Cancer Res. 36, 1–13.
Salade, L., Wauthoz, N., Vermeersch, M., Amighi, K., Goole, J., 2018. Chitosan-coated liposome dry-powder formulations loaded with ghrelin for nose-to-brain delivery. Eur. J. Pharmaceut. Biopharm. 129, 257–266.

Salama, A.H., Salama, A.A., Elhabak, M., 2021. Single step nanospray drying preparation technique of gabapentin-loaded nanoparticles-mediated brain delivery for effective treatment of PTZ-induced seizures. Int. J. Pharmaceut. 602, 120604.
Salehi, S., Nourbakhsh, M.S., Yousefpour, M., Rajabzadeh, G., Sahab-Negah, S., 2022. Chitosan-coated niosome as an efficient curcumin carrier to cross the blood–brain barrier: an animal study. J. Liposome Res. 32, 284–292.
Salem, L.H., El-Feky, G.S., Fahmy, R.H., El Gazayerly, O.N., Abdelbary, A., 2020. Coated lipidic nanoparticles as a new strategy for enhancing nose-to-brain delivery of a hydrophilic drug molecule. J. Pharmaceut. Sci. 109, 2237–2251.
Soetaert, K., 2017. plot3D: Plotting Multi-Dimensional Data, R package version 1.1. 1.
Sohail, M.F., Shahnaz, G., Ullah, N., Amin, U., Khan, G.M., Shah, K.U., 2019. Development and evaluation of optimized thiolated chitosan proniosomal gel containing duloxetine for intranasal delivery. AAPS PharmSciTech 20, 1–12.
Wang, X., Yu, Y., Ma, R., Shao, N., Meng, H., 2018. Lacosamide modulates collapsin response mediator protein 2 and inhibits mossy fiber sprouting after kainic acid-induced status epilepticus. Neuroreport 29, 1384–1390.
Zhang, C., Chanteux, H., Zuo, Z., Kwan, P., Baum, L., 2013. Potential role for human P-glycoprotein in the transport of lacosamide. Epilepsia 54, 1154–1160.
Zubairu, Y., Negi, L.M., Iqbal, Z., Talegaonkar, S., 2015. Design and development of novel bioadhesive niosomal formulation for the transcorneal delivery of anti-infective agent: In-vitro and ex-vivo investigations. Asian J. Pharmaceut. Sci. 10, 322–330.